Electronic Band Structure and Photocatalytic Activity of $Ln_2Ti_2O_7$ (Ln = La, Pr, Nd)

Dong Won Hwang,[†] Jae Sung Lee,*[,†] Wei Li,[‡] and Se Hyuk Oh[‡]

Department of Chemical Engineering, Pohang University of Science and Technology (POSTECH), San 31 Hyoja-dong, Pohang 790-784, Republic of Korea, and General Motors R&D Center

Received: January 29, 2003; In Final Form: March 20, 2003

Photocatalytic activity in the water splitting of $Ln_2Ti_2O_7$ (Ln = La, Pr, Nd) with a layered structure was highly dependent on their electronic band structure. The conduction band of $La_2Ti_2O_7$ consisted mainly of Ti 3d and La 5d, whereas the valence band consisted mainly of O 2p and Ti 3d. The empty La 4f level was found to be located ca. 3.6 eV above the bottom of the conduction band from both the electronic band-structure calculation and the XPS measurement. The occupied and unoccupied Ln 4f level in $Ln_2Ti_2O_7$ was shifted to lower energy as the number of 4f electrons increased. This shift of the Ln 4f band made it possible for the band-gap energy of both $Pr_2Ti_2O_7$ and $Nd_2Ti_2O_7$ to be decreased. For $Nd_2Ti_2O_7$, the unoccupied Nd 4f level located between the conduction band and the valence band was found to be detrimental to photocatalytic activity in water splitting because it could act as an electron-trapping site.

Introduction

Despite a number of studies about photocatalyst materials for water splitting, their reactivity−property relationship has not been well understood. Lanthanide titanites with the general formula $Ln_2Ti_2O_7$ have received much attention as a result of the observation that they might be ferroelectric by analogy with $Cd_2Nb_2O_7$, which is a unique and unusual ferroelectric material at low temperatures.[1] Among these lanthanide titanites, $La_2Ti_2O_7$ has been reported to have good photocatalytic activity in the water-splitting reaction[2,3] and in the oxidative decomposition of CH_3Cl[4] when combined with nickel oxide. In our previous paper, we concluded that its high photocatalytic activity resulted from both its layered structure and peculiar electronic structure. The perovskite slab constructing the layered structure has a hypervalency of cations (+7) that is different from that of conventional perovskite oxides (+6) such as $SrTiO_3$. In this regard, we have demonstrated that the hypervalency of the layered material is more important than the geometric layered structure in the photocatalytic water-splitting reaction. $La_2Ti_2O_7$ has a monoclinic structure with a space group of $P2_1$, and thus this compound is classified as a layered perovskite-type oxide.[5] Both neodymium titanite ($Nd_2Ti_2O_7$) and praseodymium titanite ($Pr_2Ti_2O_7$) are isostructural to $La_2Ti_2O_7$ and show ferroelectric properties and coercive fields similar to those of $La_2Ti_2O_7$.[6] It has been proposed that the peculiar geometric structure of photocatalyst materials plays a crucial role in the photocatalytic water-splitting reaction, as shown in the structures of many other photocatalysts such as the layered structure of $K_4Nb_6O_{17}$, the tunnel structure of $BaTi_4O_9$, and the pillared structure of $K_3Ta_3Si_2O_{13}$.[7−9] From this point of view, $Nd_2Ti_2O_7$ and $Pr_2Ti_2O_7$, like $La_2Ti_2O_7$, are also expected to have good photocatalytic activity because both oxides are isostructural with $La_2Ti_2O_7$, which has high photocatalytic activity. In addition, the difference in their electronic structure resulting from the different Ln 4f shell would affect their photocatalytic activity, as reported by Machida et al., who demonstrated the relationship between the photocatalytic properties and electronic structure of tantalum-based photocatalysts.[10−11]

This paper reports the results of a band-structure calculation based on the crystal structure determined by XRD and the spectroscopic characterization by XPS of $Ln_2Ti_2O_7$ (Ln = La, Pr, Nd). A correlation is sought between these band structures and photocatalytic activities for the water-splitting reaction under UV irradiation.

Experimental Section

Catalyst Preparation. $Ln_2Ti_2O_7$ (Ln = La, Pr, Nd) was synthesized from stoichiometric mixtures of oxide precursors of La_2O_3, Pr_6O_{11}, Nd_2O_3 (Alfa, 99.99%), and TiO_2 (Aldrich, anatase, 99.99%), respectively. A powder mixture was ground in mortar in the presence of EtOH and then calcined at 1123 K for 10 h followed by 1423 K for 10 h under static air conditions. Nickel was loaded on the as-prepared catalyst by a wet-impregnation method with simultaneous grinding. Thus, the prepared powder was added in aqueous or nitric acid solution containing a required amount (1.0 wt % of powder as metal) of a nickel nitrate, $Ni(NO_3)_2 \cdot 6H_2O$ (Aldrich, 99.99%). The nickel-impregnated samples were reduced by H_2 (22 μmol/s) at 773 K for 2 h and then oxidized in air (22 μmol/s) at 473 K for 1 h; these are known to be the optimum pretreatment conditions of nickel-loaded perovskite-type oxides.[3]

Characterization. The crystal structure of the sintered powder was determined with an X-ray diffractometer (Mac Science Co., M18XHF) with monochromated Cu Kα radiation at 40 kV and 200 mA. Optical properties were analyzed with a UV−vis diffuse reflectance spectrometer (Shimadzu, UV 2401). The BET surface area was evaluated by N_2 adsorption in a constant-volume adsorption apparatus (Micrometrics, ASAP 2012). The valence-band spectra were obtained from XPS measurements (VG Scientific, ESCALAB 220iXL) using Mg Kα radiation (1253.6 eV). The binding-energy calibration was performed using the C 1s peak at 284.6 eV as the reference energy.

* Corresponding author. E-mail: jlee@postech.ac.kr. Tel: 82-54-279-2006. Fax: 82-54-279-5528.
[†] Pohang University of Science and Technology (POSTECH).
[‡] General Motors R&D Center.

10.1021/jp034229n CCC: $25.00
Published on Web 05/03/2003

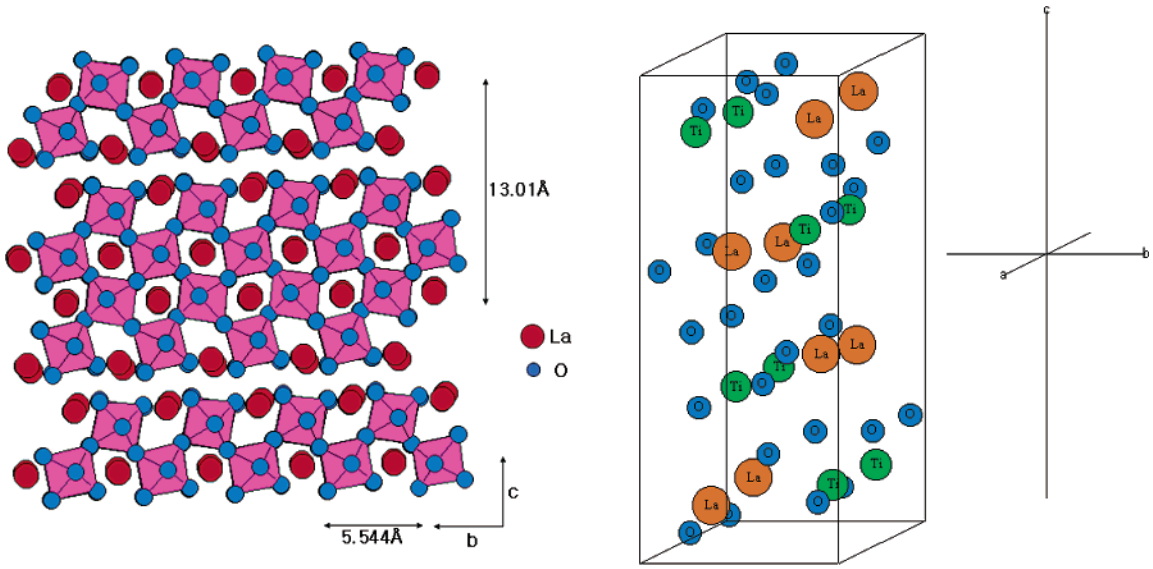

Figure 1. Schematic diagram of $La_2Ti_2O_7$ with monoclinic structure.

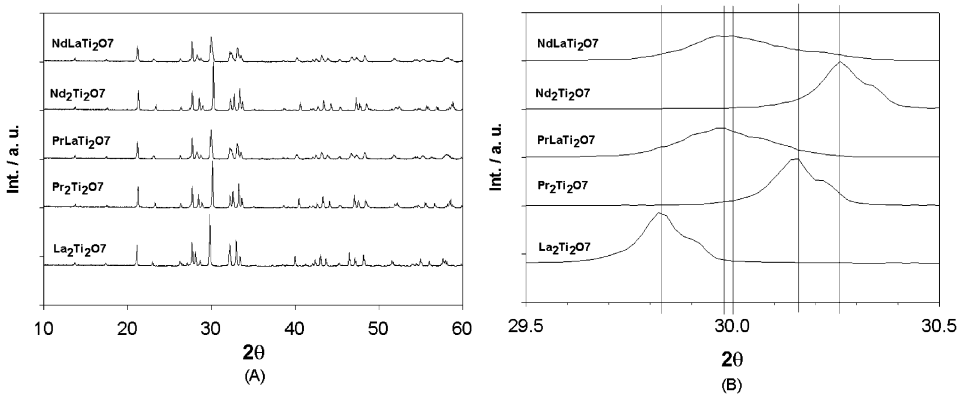

Figure 2. XRD patterns of $Ln_2Ti_2O_7$ synthesized at 1423 K for 10 h.

Band-Structure Calculation. The electronic band-structure calculation was based on the FLAPW (full potential linearized augmented plane wave) method, which uses the generalized gradient approximation (GGA), an improvement of the local spin-density approximation (LSDA) within density functional theory that is known to be an efficient and accurate scheme for solving the many-electron problem of a crystal. The Wien97 package was used in this study.[12] The crystallographic parameters including lattice parameters and atomic positions were adopted from the literature for the calculation.[13]

Photocatalytic Water-Splitting Reaction. Three types of photocatalytic reaction systems were used for testing the irradiation-dependent photocatalytic activity. For UV irradiation (>200 nm), the reaction was carried out at room temperature in a closed gas-circulation system using a high-pressure Hg lamp (Ace Glass Inc., 450 W) placed in an inner-irradiation-type quartz reaction cell. The catalyst (1.0 g) was suspended in distilled water (500 mL) by magnetic stirring. For irradiation at wavelengths longer than 360 nm, reaction was performed in an outer-irradiation-type Pyrex reactor using a high-pressure Hg lamp (Oriel, 500W). For irradiation at wavelengths longer than 420 nm, a cutoff filter (>420 nm) was placed in front of the Pyrex reactor to remove all UV irradiation. In the Pyrex reactor, the catalyst (1.0 g) was suspended in distilled water (150 mL) by magnetic stirring. The rates of H_2 and O_2 evolution were analyzed by gas chromatography (TCD, molecular sieve 5 Å column, and Ar carrier).

Results and Discussion

Crystal Structure. $La_2Ti_2O_7$ is a member of a homologous series of layered structures built from (110) perovskite slabs with the generic composition $A_mB_mO_{3m+2}$ ($m = 4, 5$; A = Ca, Sr, La; B = Ti, Nb) differing in thickness and bounded by crystallograpic shears in the perovskite [100] direction. Adjacent slabs are offset from one another by half of one TiO_6 octahedron height, and the octahedron connectivity is broken at the shear interface.[13] At room temperature, the space group of this material is $P2_1$, and the unit cell has one axis double that is observed in the alkali-metal niobates ($Ca_2Nb_2O_7$) and tantalates ($Sr_2Ta_2O_7$) (i.e., $c = 2 \times a_0$ of cubic perovskite = 7.8 Å; the shortest axis is apparently common to all members of this structural family, $b = 2^{1/2} \times a_0$ of cubic perovskite = 5.544 Å. The schematic diagram of monoclinic $La_2Ti_2O_7$ with space group of $P2_1$ is shown in Figure 1. Ti−O distances vary between 1.768 and 1.826 Å and between 2.199 and 2.288 Å. The mean value of the equatorial Ti−O distance of the four independent TiO_6 octahedra was calculated as 1.963 Å. The distances between the La atom coordinated by nine O atoms and one O atom vary between 2.464 and 2.832 Å, and the distances between the La atom coordinated by eight O atoms and one O atom vary between 2.980 and 3.286 Å.

Figure 2A shows the XRD patterns of stoichiometric mixtures of Ln_2O_3 (Ln = La, Pr, Nd) and TiO_2 sintered at 1423 K for 10 h after intermediate calcination at 1123 K for 10 h. All peaks were ascribed to the monoclinic $Ln_2Ti_2O_7$ with space group $P2_1$,

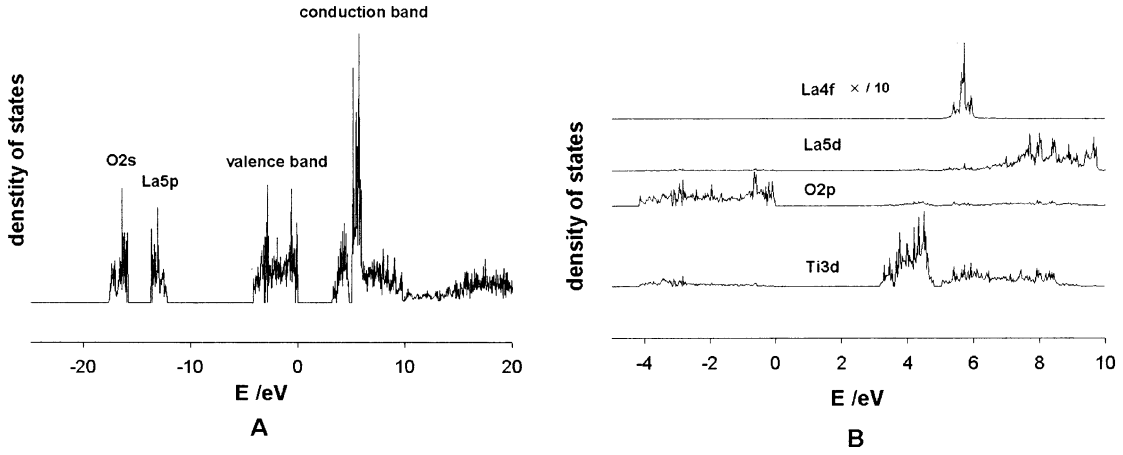

Figure 3. Density of states of $La_2Ti_2O_7$ with monoclinic structure: (A) Total DOS and (B) partial DOS of La 4f, La 5d, O 2p, and Ti 3d.

TABLE 1: Lattice Constants of $Ln_2Ti_2O_7$ (Ln = La, Pr, Nd)

lattice parameter	$La_2Ti_2O_7$	$Pr_2Ti_2O_7$	$PrLaTi_2O_7$	$Nd_2Ti_2O_7$	$NdLaTi_2O_7$
a (Å)	13.010	12.996	13.003	13.02	13.020
b (Å)	5.544	5.485	5.515	5.480	5.512
c (Å)	7.810	7.704	7.757	7.680	7.745
β (deg)	98.43	98.51	98.47	98.28	98.36
d spacing of (212) plane (Å)	2.994	2.965	2.980	2.953	2.978
V (Å^3)	557	543	551	542	550

and any impurity phases were not detectable. An expanded view of Figure 2A was shown to compare the positions of the (212) plane with the highest intensity in Figure 2B. The *d* spacing of the (212) plane followed the order of $La_2Ti_2O_7$ > $PrLaTi_2O_7$ > $NdLaTi_2O_7$ > $Pr_2Ti_2O_7$ > $Nd_2Ti_2O_7$, which was consistent with that of the ionic radius of 8-coordinated Ln^{3+} (1.30 Å, 1.27 Å, 1.25 Å for La^{3+}, Pr^{3+}, Nd^{3+}, respectively).[14]

The lattice constants of $Ln_2Ti_2O_7$ calculated from the *d* spacing of the X-ray diffraction pattern in Figure 2 are summarized in Table 1. The unit-cell volumes of $La_2Ti_2O_7$, $PrLaTi_2O_7$, $NdLaTi_2O_7$, $Pr_2Ti_2O_7$, and $Nd_2Ti_2O_7$ are 557, 551, 550, 543, and 542 Å^3, and their order is consistent with that of the *d* spacing of the (212) plane.

Band-Structure Calculation of $Ln_2Ti_2O_7$. Using crystal structure information described in the previous section, the electronic band structure of $La_2Ti_2O_7$ was calculated on the basis of the first principle calculation using the Wien97 package. The atomic coordinates for the calculation of electronic structure were adopted from the literature,[13] and lattice parameters of *a*, *b*, *c*, and β were chosen to be 13.01 Å, 5.544 Å, 7.81 Å, and 98.43°, respectively. The muffin-tin radii for La, Ti, and O were chosen to be 2.3, 1.7, and 1.6, respectively, in this calculation. The convergence parameter of RK_{max} was set to 6.0, which gave the 19 999 plane waves in the monoclinic phase. The calculation was iterated to self-consistency using interactive diagnolization with the charge convergence criterion of 0.001. The lengths of reciprocal lattice vectors were 4.926, 6.862, and 2.958. The number of mesh points in the Brillouin zone was 48, and the division of the reciprocal lattice vectors (intervals) was 462 meshes, generating 12 inequivalent *k* points.

Figure 3A shows the total density of states (DOS) of monoclinic $La_2Ti_2O_7$, where the top of the valence band was set to 0 eV. It is seen clearly from this DOS plot that this material has an insulating property because there exists a large band-gap between the valence and conduction bands. The core band exists from −18 to −12 eV, which consists of mainly O 2s and La 5p. The valence band exists from −4 to 0 eV, and the main portion of the conduction band exists from 3.2 to 10 eV, although the continuous band exists even at energy higher than 10 eV because of the unoccupied O 2p. The band-gap energy between the valence band (VB) and the conduction band (CB) was about 3.2 eV, which is a little underestimated. This underestimation comes from some flaws in the generalized gradient approximation (GGA) used for this calculation. The valence band consists of mainly O 2p, which is hybridized a little with Ti 3d, as shown in Figure 3B. This means that some portion of Ti 3d takes part in the interaction with O 2p to construct the valence band. Conversely, the conduction band consists of mainly Ti 3d covering from 3.2 to 9 eV, which split into two distribution bands at 3.2 to 4.8 eV and 4.8 to 9 eV as a result of crystal-field splitting in the octahedral TiO_6 environment. The contribution of La atoms to the bands of Ti 3d and O 2p is very small because of the large distance between La and Ti or La and O atoms. Instead, La 4f and La 5d, which are unoccupied and localized a little, contribute greatly to the conduction band. An unoccupied sharp La 4f orbital covers the conduction band at an energy level from 5 to 6 eV, which is almost localized from the Ti 3d and O 2p orbitals. As expected, the La 4f orbital did not contribute to the valence band because there is no electron that occupies the La 4f shell. La 5d covers the latter part of the conduction band from 7 to 10 eV, which is a little overlapped but not hybridized with Ti 3d, as judged from the different band shape. The O 2p orbital also contributes a little to the conduction band and splits into two energy states like Ti 3d does, which also reflects the fact that there is some electronic interaction between O 2p and Ti 3d constructing the conduction band of $La_2Ti_2O_7$.

As seen in Figure 4, the electronic structures of four inequivalent La atoms are not so different from each other because the average distance between the La and O atom is similar, although the interatomic distance within the individual La atom varies greatly, as shown in Figure 1. The partial DOSs of four inequivalent Ti and O atoms are also not so different, which might result from the similar interatomic distance between the Ti and O atoms. Figure 5 shows the electronic band structure with the band character of monoclinic $La_2Ti_2O_7$. The valence band from −4 to 0 eV and the conduction band from 3.2 to 10 eV are shown clearly from this plot. In addition, it is clear from this band structure that the band gap appears between the highest point of the valence band and the lowest point of the conduction band at the same Γ point. Therefore, a direct optical transition can occur with no significant change in the wave vector for this compound. This direct band gap is one of the desirable properties of photocatalyst materials because light absorption

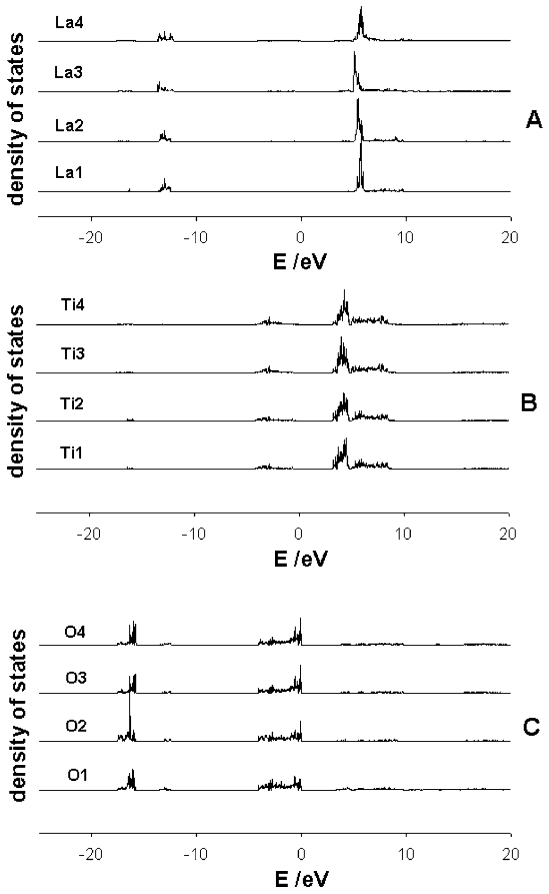

Figure 4. Partial density of states of the individual atoms: (A) La, (B) Ti, (C) O.

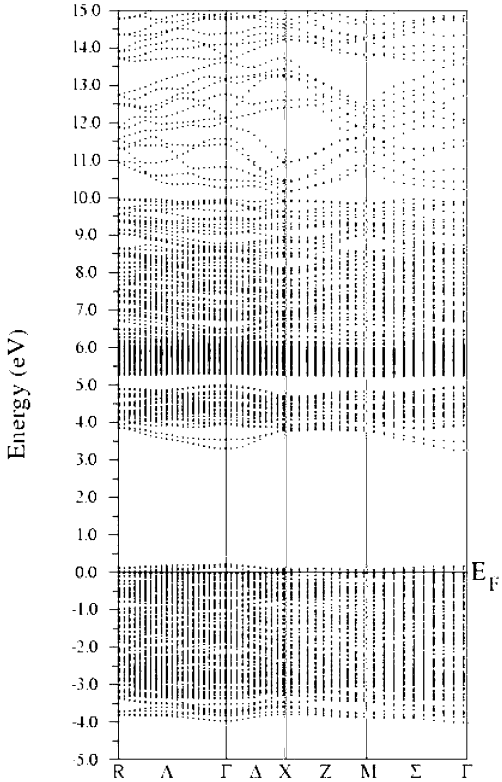

Figure 5. Electronic band structure of monoclinic $La_2Ti_2O_7$.

for this kind of materials can occur more efficiently compared with that for materials with the indirect band gap.

We also calculated the electronic structure of TiO_2 with the rutile structure for comparison with that of $La_2Ti_2O_7$. As shown in Figure 6, the band-gap energy from this calculation was about 2.0 eV, which is an overly underestimated value compared with the experimental band-gap energy of 3.2 eV. The conduction band of TiO_2 with the rutile structure consists of mainly Ti 3d and a little O 2p, whereas the valence band consists of mainly O 2p and a little Ti 3d. It is noticeable that the shapes of O 2p and Ti 3d are very similar, which reflects considerable hybridization between O 2p and Ti 3d in both the valence and conduction bands. Although $La_2Ti_2O_7$ also shows some hybridization of Ti 3d with O 2p, the degree of hybridization was much less than that of TiO_2. This is because the distances are nearly the same between Ti and 6-neighbored O atoms in TiO_2 with rutile structure at ca. 1.0 Å. However, Ti−O distances in $La_2Ti_2O_7$ vary between 1.768 and 1.826 Å and between 2.199 and 2.288 Å, and the mean value of the equatorial Ti−O distance of the four independent TiO_6 octahedra was calculated to be 1.963 Å, as mentioned earlier. The width of the conduction band of $La_2Ti_2O_7$ is 6.8 eV, which is a little larger than that of TiO_2 (5.8 eV) because of the La 5d band located in the upper part of the conduction band. In addition, the conduction-band edge was shifted to a higher energy by La addition to TiO_2.

UV−Visible Diffuse Reflectance Spectroscopy (Optical Property). Figure 7 shows the UV−vis DRS patterns of $Ln_2Ti_2O_7$ (Ln = La, Pr, Nd) synthesized by solid-state reactions of La_2O_3, Pr_6O_{11}, Nd_2O_3, and TiO_2 at 1423 K for 10 h. The colors of native $La_2Ti_2O_7$ (A), $NdLaTi_2O_7$ (B), $Nd_2Ti_2O_7$ (C), $PrLaTi_2O_7$ (D), and $Pr_2Ti_2O_7$ (E) were colorless, light green, green, light violet, and violet, respectively. Any absorption originating from other impurities or unreacted precursor oxides was not detected. Visible-light absorption at wavelength longer than 420 and 350 nm was observed for Pr- and Nd-containing $Ln_2Ti_2O_7$, respectively. These visible-light absorptions could be ascribed to the internal transitions in a partially filled Ln 4f shell and are in accord with those of Ln(III) hexahalide complexes and simple sequioxides.[15] Another absorption for all compounds was observed at wavelengths shorter than the absorption edges corresponding to the internal 4f transitions. These band-gap transitions showed red shifts when Pr or Nd was substituted for La in $Ln_2Ti_2O_7$. The band-gap absorption edges and band-gap energies calculated from the absorption-edge positions of these materials are summarized in Table 2. The order of the band-gap energies of $Ln_2Ti_2O_7$ is $La_2Ti_2O_7$ (3.82 eV) > $NdLaTi_2O_7$ (3.68 eV) ≈ $Nd_2Ti_2O_7$ (3.65 eV) > $Pr_2Ti_2O_7$ (2.99 eV) ≈ $PrLaTi_2O_7$ (2.98 eV). The band-gap energy is highly dependent on the number of Ln 4f electrons, which showed a minimum for $Pr_2Ti_2O_7$ with three 4f electrons ($[Xe]4f^36s^2$), and both $Nd_2Ti_2O_7$ with four 4f electrons ($[Xe]4f^46s^2$) and $La_2Ti_2O_7$ without 4f electrons ($[Xe]5d^16s^2$) showed larger values. The mixed lanthanides ($PrLaTi_2O_7$ and $NdLaTi_2O_7$) showed a similar band-gap energy to that of the single lanthanides ($Pr_2Ti_2O_7$ and $Nd_2Ti_2O_7$), but the absorption intensity of the mixed lanthanide was somewhat lowered because the concentration of Pr or Nd was decreased. This band-gap dependence on the number of f electrons of the lanthanide was also observed for $LnTaO_4$ and Ln_3TaO_7, where the band-gap energies of $PrTaO_4$ and Pr_3TaO_7 were the lowest in each series except for those of $CeTaO_4$ and Ce_3TaO_7.[10]

Photocatalytic Activity. For all photocatalysts reported here, $Ln_2Ti_2O_7$ with monoclinic structure showed good activity for the photocatalytic decomposition of water into H_2 and O_2 under UV irradiation. In addition to these high activities, H_2 and O_2 were produced in a stoichiometric ratio (H_2/O_2 = 2:1), and there

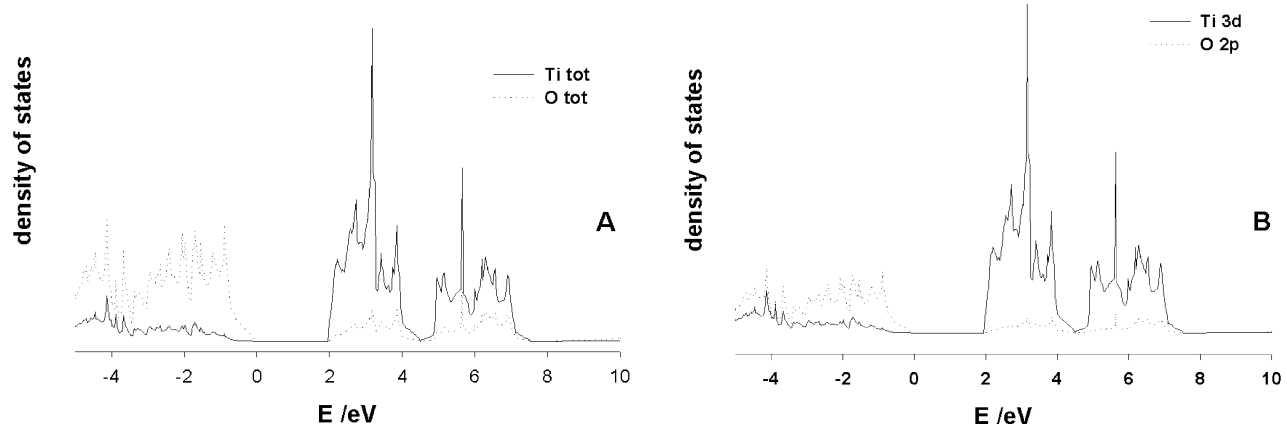

Figure 6. Density of states of TiO_2 with rutile structure: (A) Partial DOS of Ti and O, (B) partial DOS of Ti 3d and O 2p.

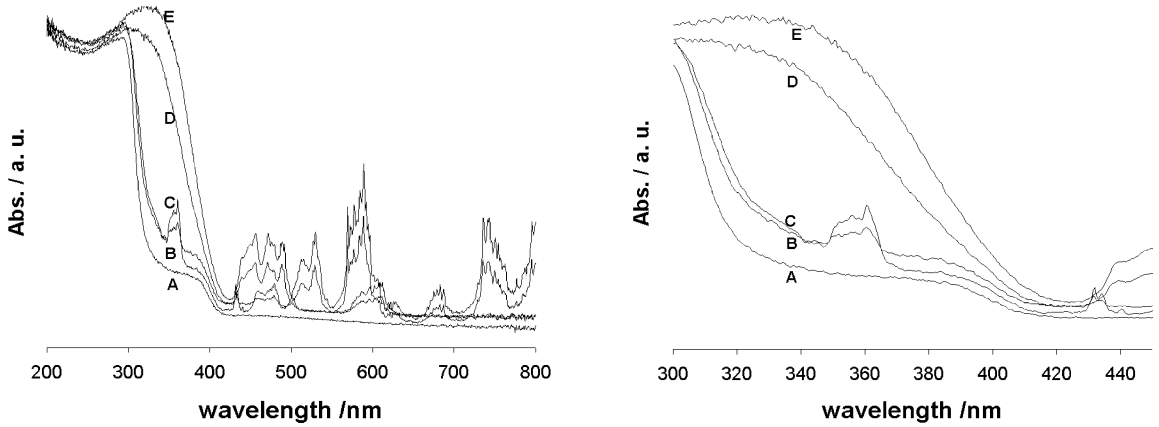

Figure 7. UV−vis diffuse reflectance spectra of $Ln_2Ti_2O_7$ (Ln = La, Pr, Nd): (A) $La_2Ti_2O_7$, (B) $NdLaTi_2O7$, (C) $Nd_2Ti_2O_7$, (D) $PrLaTi_2O_7$, (E) $Pr_2Ti_2O_7$. All catalysts were sintered at 1423 K for 10 h.

TABLE 2: Optical Properties of $Ln_2Ti_2O_7$ (Ln = La, Pr, Nd)

material	absorption edge (nm)	band-gap energy (eV)
$La_2Ti_2O_7$	325	3.82
$Pr_2Ti_2O_7$	415	2.99
$PrLaTi_2O_7$	416	2.98
$Nd_2Ti_2O_7$	340	3.65
$NdLaTi_2O_7$	337	3.68

was no indication of catalyst deactivation for 20 h, during which time the catalyst had turned over many times, making the overall process of water splitting catalytic. The typical time courses of H_2 and O_2 evolution over nickel-loaded $La_2Ti_2O_7$ are shown in Figure 8.

Photocatalytic activities of $Ln_2Ti_2O_7$ in the water-splitting reaction are summarized in Table 3. All native oxides showed very low activity (less than 10 μmol H_2/h g_{cat}) under irradiation of light with wavelengths longer than 200 nm, corresponding to 6.2 eV. When irradiation was limited to wavelengths longer than 360 nm, no materials showed any activity. Even $Pr_2Ti_2O_7$ and $PrLaTi_2O_7$, which have an absorption edge of ca. 415 nm and thus could absorb sufficient energy from this irradiation for the excitation of electrons in the valence band, did not produce any H_2 from pure water. This means that electron−hole recombination could take place excessively over these semiconductor photocatalysts, and thus most of the charge carriers generated by light absorption at wavelengths longer than 360 nm would not be transferred to the reactant molecule (H^+ or OH^-) on the surface. Nickel oxide loading on perovskite-type oxide followed by reduction and reoxidation is the well-known process for the activation of photocatalyst materials, especially in the water-splitting reaction. When nickel oxide was loaded on $Ln_2Ti_2O_7$, the H_2 evolution rate under irradiation at wavelengths longer than 200 nm increased significantly for all compounds. The role of nickel on the external surface of these materials is thought to be the construction of a p−n junction between nickel oxide and perovskite-type materials, over which more effective charge separation of electron−hole pairs could take place.[16] It is noticeable that for $La_2Ti_2O_7$ a

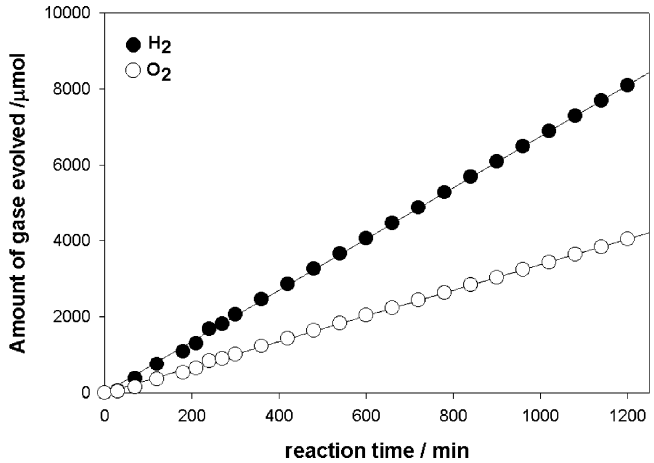

Figure 8. Typical time courses of H_2 and O_2 evolution over Ni(1.0 wt %)/$La_2Ti_2O_7$. The catalyst was pretreated by reduction at 773 K for 2 h followed by oxidation at 473 K for 1 h. Reaction conditions: catalyst, 1 g; distilled water, 500 mL; light source, 450-W high-pressure Hg lamp placed in the inner-irradiation reaction cell.

TABLE 3: Photocatalytic Activity of $Ln_2Ti_2O_7$

material	activity (amount of H_2 (μmole/h g_{cat}) [a]inner irradiation (λ > 200 nm)	[b]outer irradiation (λ > 360 nm)	[c]outer irradiation (λ > 420 nm)
$La_2Ti_2O_7$	10	0	0
[d]$NiO_x/La_2Ti_2O_7$	400	0	0
$Pr_2Ti_2O_7$	5	0	0
$NiO_x/Pr_2Ti_2O_7$	150	30	0
$PrLaTi_2O_7$	8	0	0
$NiO_x/PrLaTi_2O_7$	220	20	0
$Nd_2Ti_2O_7$	4	0	0
$NiO_x/Nd_2Ti_2O_7$	99	0	0
$NdLaTi_2O_7$	6	0	0
$NiO_x/NdLaTi_2O_7$	131	0	0

[a] Measured in an inner-irradiation quartz reaction cell under irradiation from a 450-W high-pressure Hg lamp; H_2O 500 mL, catalyst 1.0 g. [b] Measured in outer-irradiation cell from a 500-W high-pressure Hg lamp; H_2O 150 mL, catalyst 1.0 g. [c] Measured in outer-irradiation cell from a 500-W high-pressure Hg lamp; H_2O 150 mL, catalyst 1.0 g, 420-nm cutoff filter. [d] Materials were loaded with Ni (1.0 wt %) and then pretreated by reduction at 773 K for 2 h followed by oxidation at 473 K for 1 h.

remarkable increase in the water-splitting activity by loading nickel oxide was observed. The BET surface area of all compounds was about 1 m^2/g because of the preparation at a high temperature of 1423 K for 10 h. Therefore, other factors governing the photocatalytic activity in water splitting should be considered to explain the variation of photocatalytic activity among various compounds because all materials in the present study have the same layered structure composed of TiO_6 octahedra. When La was substituted for Pr and Nd in $Pr_2Ti_2O_7$ and $Nd_2Ti_2O_7$, respectively, photocatalytic activity under full irradiation (λ > 200 nm) was increased ($PrLaTi_2O_7$ > $Pr_2Ti_2O_7$; $NdLaTi_2O_7$ > $Nd_2Ti_2O_7$). However, when irradiation was limited to wavelengths longer than 360 nm, only $NiO_x/Pr_2Ti_2O_7$ and $NiO_x/PrLaTi_2O_7$ were found to be active. This might be ascribed to their band-gap energy, as shown in the UV−vis diffuse reflectance spectra of Figure 7, where only these two compounds could absorb light of wavelengths longer than 360 nm. Under this irradiation, the photocatalytic activity of $PrLaTi_2O_7$ was somewhat lower than that of $Pr_2Ti_2O_7$ (30 vs 20 μmol H_2/h g_{cat}). No activity was observed under irradiation at wavelengths longer than 420 nm because the absorption edges of both $Pr_2Ti_2O_7$ and $PrLaTi_2O_7$ (415 and 416 nm, respectively) were shorter than 420 nm.

Valence-Band XPS Spectra. To find the energy level of the valence band of each compound, XPS measurements were made especially for the valence-band region, as shown in Figure 9. $La_2Ti_2O_7$ (spectrum A) showed only one broad peak (6.7 eV) ranging from 10 to 2 eV, which was ascribed to the valence band consisting mainly of O 2p hybridized a little with Ti 3d because the contribution of the La atom to the valence band was negligible for $La_2Ti_2O_7$, as shown in the electronic band structure of $La_2Ti_2O_7$ in Figure 3. The valence-band width of $La_2Ti_2O_7$ (8 eV) was about 2 times larger than that from the electronic structure calculation (4 eV). The peak at ca. 16 eV (not shown) was assigned to La 5p, which was also consistent with the result of the electronic structure calculation. For $Pr_2Ti_2O_7$ (B), another shoulder peak (3.4 eV) with an edge energy of ca. 1 eV was observed, besides a peak originating from O 2p. The intensity of this shoulder peak was diminished as the concentration of Pr decreased, as shown by the spectrum of $PrLaTi_2O_7$ in Figure 9C. For $Pr_2Ti_2O_7$, the edge energy of the partially filled Pr 4f would be located 1.0 eV above the top of the valence band of $La_2Ti_2O_7$, and thus the total valence band

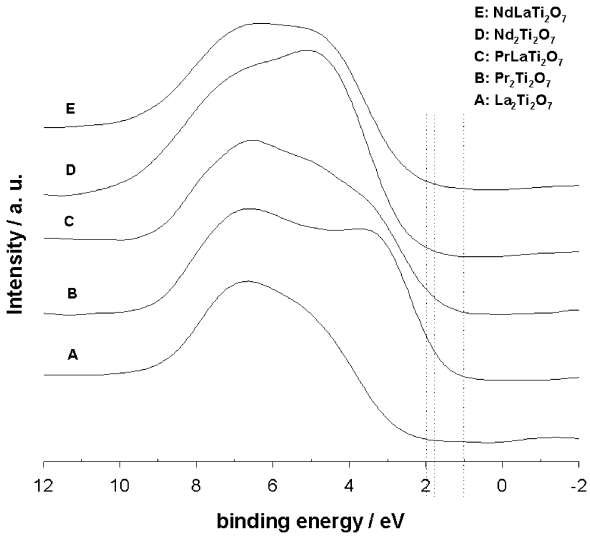

Figure 9. Valence-band spectra of $Ln_2Ti_2O_7$ (Ln = La, Pr, Nd): (A) $La_2Ti_2O_7$, (B) $Pr_2Ti_2O_7$, (C) $PrLaTi_2O_7$, (D) $Nd_2Ti_2O_7$, (E) $NdLaTi_2O_7$. All catalysts were sintered at 1423 K for 10 h.

of $Pr_2Ti_2O_7$ would be expanded from 6 to 7 eV compared with that of $La_2Ti_2O_7$. For $Nd_2Ti_2O_7$ (D), this shoulder peak (5.0 eV) with an edge position of 1.8 eV was shifted to higher energy compared with that of $Pr_2Ti_2O_7$, which was consistent with the relative energy level of the partially filled Nd 4f and Pr 4f orbitals. From this valence-band spectra, it can be concluded that the order of the top of the valence band was as follows: $La_2Ti_2O_7$ > $Nd_2Ti_2O_7$ > $Pr_2Ti_2O_7$. For $PrLaTi_2O_7$ and $PrNdTi_2O_7$, the top of the valence band was same with $Pr_2Ti_2O_7$ and $Nd_2Ti_2O_7$, respectively, and it was found that the difference in the band-gap energy with different Ln atoms in $Ln_2Ti_2O_7$ results mainly from the different shape of the valence band of each compound.

Band-Structure Model of $Ln_2Ti_2O_7$. As shown in the electronic structure calculation of $La_2Ti_2O_7$, the conduction band consists mainly of broad Ti 3d and sharp La 4f orbitals, whereas the valence band consists mainly of O 2p. The valence-band spectrum of $La_2Ti_2O_7$ from XPS showed that there was no contribution of La to the valence band and that the top of the valence band was located ca. 2 eV below the Fermi energy level. In addition, it was found that the width of the valence band was 8 eV. The UV−vis DRS of $La_2Ti_2O_7$ shown in Figure 7 revealed a single absorption edge corresponding to 3.82 eV, which means that any other energy states would not exist between the valence and conduction bands. The width of the valence band was just 4 eV from the band-structure calculation, and thus if we calibrate this value with the experimental one of 8 eV, the width of the real conduction band would be about 12 eV. The empty and highly localized La 4f orbital is positioned ca. 3.6 eV above the bottom of the conduction band. Therefore, the band structure of $La_2Ti_2O_7$ can be depicted schematically as shown in Figure 10A. For $Pr_2Ti_2O_7$ and $Nd_2Ti_2O_7$, however, it was impossible to obtain the band structure from the direct calculation of the electronic structure. The partially filled Pr 4f and Nd 4f orbitals did not split into occupied and unoccupied states. Thus, the Fermi level was pinned at the 4f band and finally the calculated electronic structure did not reflect the insulating property of $Pr_2Ti_2O_7$ and $Nd_2Ti_2O_7$. However, it is easily expected that the Ln 4f level of $Ln_2Ti_2O_7$ would shift to lower energy with an increase in the number of 4f electrons because the same trend was observed for the electronic structures of $LnTaO_4$ and $RbLnTa_2O_7$.[10,11] The band-gap energy of $Pr_2Ti_2O_7$ was found to be 2.99 eV from the light-absorption edge,

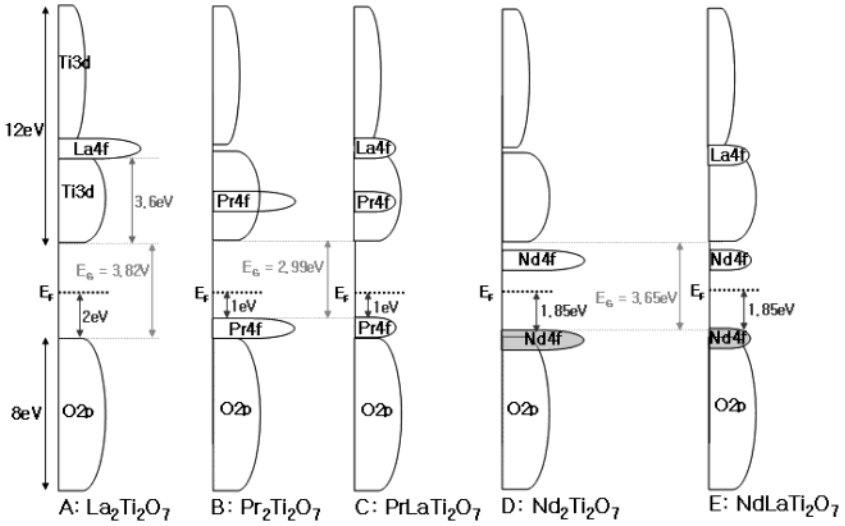

Figure 10. Band-structure model of $Ln_2Ti_2O_7$ (Ln = La, Pr, Nd).

and the top of the valence band was located ca. 1 eV below the Fermi level; the width of the valence band was ca. 9 eV from the valence-band spectrum. The unoccupied Pr 4f would still be located at an energy higher than the bottom of the conduction band; finally, the whole band structure of $Pr_2Ti_2O_7$ could be depicted as Figure 10B. For $PrLaTi_2O_7$, the band structure would be more complex than that of $Pr_2Ti_2O_7$. For $PrLaTi_2O_7$, the band-gap energy was similar to that of $Pr_2Ti_2O_7$, but the intensity of the valence band at lower binding energy (ca. 3.4 eV) was decreased, which resulted from the decrease in the overlapping of the occupied Pr 4f with O 2p for $PrLaTi_2O_7$. Therefore, the band structure of $PrLaTi_2O_7$ was described as Figure 10C. For $Nd_2Ti_2O_7$, the top of the valence band was located 1.85 eV below the Fermi level, which implied that the occupied Nd 4f was 0.15 eV above O 2p. The band-gap absorption corresponding to 3.65 eV observed in the UV−vis spectrum in Figure 7 was ascribed to the transition from the valence band (O 2p overlapped with occupied Nd 4f) to the conduction band (Ti 3d). The unoccupied Nd 4f would be located at a lower energy than the unoccupied Pr 4f and would lie between the conduction band and the valence band, as seen for $RbLnTa_2O_7$.[11] Therefore, the band structure of $Nd_2Ti_2O_7$ was described as Figure 10D. The band structure of $NdLaTi_2O_7$ can be as Figure 10E because the intensity of the valence band corresponding to the occupied Nd 4f was decreased.

Relationship between the Photocatalytic Activity and Band Structure of $Ln_2Ti_2O_7$. As compared in Table 3, the photocatalytic activity of $Ln_2Ti_2O_7$ and nickel-loaded $Ln_2Ti_2O_7$ varied markedly with the type of Ln (Ln = La, Pr, Nd) constructing $Ln_2Ti_2O_7$ with a layered structure, although the variation for the native compounds was less than that for nickel-loaded ones. The order of photocatalytic activity for the water-splitting reaction can be summarized as follows: $La_2Ti_2O_7 \gg PrLaTi_2O_7 > Pr_2Ti_2O_7 > NdLaTi_2O_7 > Nd_2Ti_2O_7$. The origin of the difference in the photocatalytic activity of $Ln_2Ti_2O_7$ seems to be closely related to its relative electronic band structure because all of the compounds have the same layered perovskite-type structure. The peculiar higher activity of $La_2Ti_2O_7$ compared with that of other compounds was ascribed to the location of the empty La 4f at a higher energy level compared with those of Pr 4f and Nd 4f. For efficient photocatalysis, electron−hole pairs should be separated energetically as well as geometrically. The band structure of $La_2Ti_2O_7$ appears to be very desirable for charge separation because any potential trapping site between the valence and conduction bands does not exist. In addition, the relatively higher band-gap energy (3.82 eV) of $La_2Ti_2O_7$ could also be responsible for the good photocatalytic activity. The reason that $Pr_2Ti_2O_7$ had a lower activity than $La_2Ti_2O_7$ under full irradiation was thought to be the reduction of the band gap, which resulted from the occupied Pr 4f band located ca. 1 eV above the O 2p band, as shown in Figure 10B. Therefore, the smaller band gap is not advantageous for the suppression of electron−hole recombination. For $Pr_2Ti_2O_7$, H_2 was also observed, even under irradiation with wavelengths longer than 360 nm, which meant that the occupied Pr 4f orbital, not the occupied O 2p orbital, was used for this reaction. When La was substituted for Pr in $Pr_2Ti_2O_7$, the activity was increased under full irradiation ($\lambda > 200$ nm), which was consistent with the result that $La_2Ti_2O_7$ had a higher activity than $Pr_2Ti_2O_7$. However, the substitution of La for Pr resulted in a lowering of the photocatalytic activity under the irradiation of light with wavelengths longer than 360 nm. This was ascribed to the decrease of the concentration in the Pr 4f because only the electrons from the occupied Pr 4f band could be excited to the conduction band under the irradiation of light with wavelengths longer than 360 nm. The lowest photocatalytic activity of $Nd_2Ti_2O_7$ was ascribed to the empty Nd 4f level ca. 1 eV below the conduction band (D), which could play a crucial role in trapping the excited electrons. The electrons trapped at the empty Nd 4f level would not be able to reach the catalyst surface because of its strongly localized character, which resulted in a lowering of the photocatalytic activity of $Nd_2Ti_2O_7$. When La was substituted for Nd in $Nd_2Ti_2O_7$, the concentration of the unoccupied Nd 4f was decreased (E), which would result in a higher activity of $LaNdTi_2O_7$ compared with that of $Nd_2Ti_2O_7$.

Conclusions

The present study revealed that photocatalytic activity is highly dependent on the electronic band structure as well as on the bulk structure of photocatalyst materials. The Ln 4f level in $Ln_2Ti_2O_7$ was shifted to lower energy as the number of Ln 4f electrons increased. This red shift of the Ln 4f band made it possible for the band-gap energy of both $Pr_2Ti_2O_7$ and $Nd_2Ti_2O_7$ to be decreased. For $Nd_2Ti_2O_7$, the unoccupied Nd 4f level located between the conduction and valence bands was found to be detrimental to photocatalytic activity in water splitting by providing electron-trapping sites.

Acknowledgment. This work was supported by the General Motors R & D Center, the Brain Korea 21 project, and the Research Center for Energy Conversion and Storage.

References and Notes

(1) Prasadarao, A. V.; Selvaraj, U.; Komarneni, S. Bhalla, A. S. *J. Mater. Res.* **1992**, *7*, 2859.

(2) Kim, H. G.; Hwang, D. W.; Kim, J.; Kim, Y. G.; Lee, J. S. *Chem. Commun*. **1999**, 1077.

(3) Hwang, D. W.; Kim, H. G.; Kim, J.; Cha, K. Y.; Kim, Y. G.; Lee, J. S. *J. Catal*. **2000**, *193*, 40.

(4) Hwang, D. W.; Cha, K. Y.; Kim, J.; Kim, H. G.; Bae, S. W.; Lee, J. S. *Ind. Eng. Chem. Res*. **2003**, *42*, 1184.

(5) Ishizawa, N.; Marumo, F.; Kawamura, T.; Kimura, M. *Acta Crystallogr., Sect. B* **1975**, *31*, 1912.

(6) Prasadarao, A. V.; Selvaraj, U.; Komarneni, S.; Bhalla, A. S. *Mater. Lett*. **1991**, *12*, 306.

(7) Domen, K.; Kudo, A.; Onishi, T. *J. Catal*. **1986**, *102*, 92.

(8) Inoue, Y.; Asai, Y.; Sato, K. *J. Chem. Soc., Faraday Trans*. **1994**, *90*, 797.

(9) Kudo, A.; Kato, H. *Chem. Lett*. **1997**, 867.

(10) Machida, M.; Murakami, S.; Kijima, T.; Matsushima, S.; Arai, M. *J. Phys. Chem. B* **2001**, *105*, 3189.

(11) Machida, M.; Yabunaka, J.; Kijima, T.; Matsushima, S.; Arai, M. *Int. J. Inorg. Mater*. **2001**, *3*, 545.

(12) Blaha, P.; Schwarz, K.; Luitz, J. *WIEN97: A Full Potential Linearized Augmented Plane Wave Package for Calculating Crystal Properties;* Techn. Universität Wien: Wien, Austria, 1999.

(13) Schmalle, H. W.; Williams, T.; Reller, A.; Linden, A.; Bednorz, J. G. *Acta Crystallogr., Sect. B* **1993**, *49*, 235.

(14) Huheey, J. E.; Keiter, E. A.; Keiter, R. L. *Inorganic Chemistry: Principles of Structure and Reactivity*, 4th ed.; HarperCollins College Publishers: New York, 1993.

(15) Ryan, J. L.; Jørgensen, C. K. *J. Phys. Chem.* **1966**, *70*, 2845.

(16) Domen, K.; Naito, S.; Soma, M.; Ohnishi, T.; Tamaru, K.; *J. Chem. Soc., Chem. Commun*. **1980**, 543.